Research Article

Hossein Bayat, Mohammad Fasihi*, Yasser Zare, and Kyong Yop Rhee*

An experimental study on one-step and two-step foaming of natural rubber/silica nanocomposites

https://doi.org/10.1515/ntrev-2020-0032
received December 25, 2019; accepted January 02, 2020

Abstract: The curing and cellular structure of natural rubber (NR)/silica composite foams were investigated. The presence of an activator in the rubber formulation significantly lowered the decomposition temperature of the azodicarbonamide foaming agent, which allowed foaming before NR curing. Therefore, two foam methods were designed: foaming initially at 90°C and then curing at 140°C, and foaming and curing simultaneously at 140°C. Two-step foaming generated a lower cell density and higher cell size. Incorporation of nano silica into NR increased the foam density, but decreased the cell size. The higher foaming temperature restricted the bubble growth because of a higher curing rate and inhibited cell coalescence.

Keywords: foam, natural rubber (NR), nanosilica, cellular morphology, curing

1 Introduction

Nanomaterials have received widespread attention for numerous applications [1–26]. Additionally, there is a critical need for solid materials, which simultaneously provide the processing of polymers and the high electrical properties of metals [27–38]. Today, polymeric foams have attracted much attention from different industries. Elastomeric foams have greater flexibility than plastic foams, and thus, they are applied in specific uses such as soft insulation. The properties of foams are influenced by their density and cellular structure, which in turn is governed by the foaming process and conditions [39]. The foaming of rubber is most often conducted by physical or chemical techniques. The control of cell size and cell distribution in rubber foams is more challenging than in thermoplastic foams since simultaneous foaming and curing occur [40–42]. Therefore, a balance between foaming and curing progress is essential. In the chemical method, bubble growth and curing are developed by heating. Consequently, suitable thermal conditions should be determined.

Commercially available rubber foams are produced from ethylene propylene diene monomer rubber (EPDM), styrene-butadiene rubber (SBR), acrylonitrile-butadiene rubber (NBR), natural rubber (NR), and polyurethane (PU). NR-based foams have exceptional properties such as low-temperature flexibility, excellent tear strength, and very good resilience [43,44]. Several studies have been performed on the properties and performance of NR foams. In most studies in this field, NR latex was used to produce foam [45,46]. However, a limited number of studies have been reported on the preparation of foams from solid NR. Najib *et al.* investigated mechanical performance and sound absorption of NR foams [47]. The foams with smaller cell sizes displayed higher sound absorption performance. Similar work on these properties was performed by Harnnarongchai [48]. The impact of temperature and rubber type on the properties of NR foams was also reported [49]. Moreover, it was stated that adding carbon black decreased the cell size and increased the cell density of NR foams [44,50]. The impact of blowing agent content on cure characteristics and mechanical and morphological properties of NR foams was reported by Pechurai et al. [51] who used

* **Corresponding author: Mohammad Fasihi,** School of Chemical, Petroleum and Gas Engineering, Iran University of Science and Technology, Tehran 16846-13114, Iran, e-mail: mfasihi@iust.ac.ir
* **Corresponding author: Kyong Yop Rhee,** Department of Mechanical Engineering, College of Engineering, Kyung Hee University, Yongin 446-701, Republic of Korea, e-mail: rheeky@khu.ac.kr
Hossein Bayat: School of Chemical, Petroleum and Gas Engineering, Iran University of Science and Technology, Tehran 16846-13114, Iran
Yasser Zare: Department of Mechanical Engineering, College of Engineering, Kyung Hee University, Yongin 446-701, Republic of Korea

4,4′-oxydibenzenesulfonyl hydrazide (OBSH) as a foaming agent. Additionally, a combination of amino alcohol and carbonic acid [52] and a combination of sodium bicarbonate and azodicarbonamide were also considered as blowing agents [53,54]. A high level of the blowing agent led to more cell coalescence [54]. The effect of adding silica nanofiller on the curing and cellular structure of NR foams has been studied in our previous work [55,56]. It was found that the curing system of NR acted as an efficient activator for the blowing agent and promoted its decomposition. In addition, the blowing agent in the formulation of NR can promote the curing rate because of its exothermic decomposition. This finding allowed us to design one-step and two-step foaming processes, which were not studied in our previous work.

In this work, the cellular characteristics of one-step and two-step foaming were compared. In the one-step route, foaming and curing were performed simultaneously at 140°C. In the two-step route, foaming was performed at 90°C and curing was accomplished at 140°C. Moreover, the effect of incorporated silica particles was investigated.

2 Materials and methods

2.1 Materials

Natural rubber (NR) ribbed smoked sheet 1 (RSS1) as the matrix was supplied by Thomson Enterprise Co. (India). Precipitated silica (ULTRASIL VN3) was purchased from Evonik Industries (Germany) as nanofiller with a specific surface area of 180 m^2/g and an average particle size of 15 nm. Tetramethyl thiuram disulfide (TMTD) and *N*-cyclohexyl-2-benzothiazole sulfonamide (CBS) as accelerators and activated *azodicarbonamide* (porofor ADC/K) as the blowing agent were received from Lanxess Co. (Germany). Zinc oxide (ZnO) as the activator, sulfur as the curing agent, stearic acid, and paraffin oil were obtained from local companies.

2.2 Compounding of samples

The mixing of components was performed by an internal compounder (Brabender W50 EHT) at 60°C at a rotating speed of 80 rpm. First, NR was added into the mixer, and then silica and paraffin oil were gradually added within about 4 min. Subsequently, other ingredients consisting of the activator, accelerators, sulfur, blowing agent, and stearic acid were added into the mixer. The total mixing time for all samples was set at 15 min. Sample codes and compositions are introduced in Table 1.

2.3 Foam preparation

Two routes for preparing NR foams were designed. In the one-step method (route 1), foaming and curing of samples were conducted at 140°C for 20 min in a hot oven. The samples were cooled at room temperature after foaming. In the two-step method (route 2), first foaming was conducted for 10 min at 90°C, and then curing was performed at 140°C for 20 min using a hot oven.

2.4 Characterizations

An oscillating disc rheometer (ODR; Hiwa 100, Iran) was used to measure the rheology of the samples at temperatures of 90°C and 140°C in accordance with the ASTM D2084. Foam density was determined by the displacement method according to the ASTM D792. Scanning electron microscopy (SEM; VegaII Tescan, Czech) was applied to analyze the cell morphology. Samples were coated before this test with a thin layer of gold for better resolution. The average cell size of the bubbles was calculated by the ImageJ software from at least 50 different cell measurements.

Table 1: Compositions of prepared samples

Samples code	NR (phr)[a]	Stearic acid (phr)	Sulfur (phr)	ZnO (phr)	TMTD (phr)	CBS (phr)	Oil (phr)	Silica (phr)	Foaming agent (phr)
PR	100	2	0.5	4	2.5	1	40	0	0
S0	100	2	0.5	4	2.5	1	40	0	8
S10	100	2	0.5	4	2.5	1	40	10	8
S20	100	2	0.5	4	2.5	1	40	20	8
S30	100	2	0.5	4	2.5	1	40	30	8
S40	100	2	0.5	4	2.5	1	40	40	8

[a] phr: part per hundred of rubber (g/g).

The cell density of foams was determined using equation (1):

$$N = \frac{6}{\pi d^2}\left(\frac{\rho_r}{\rho_f} - 1\right) \quad (1)$$

where N is the cell density, d is the cell size (diameter), ρ_r is the solid rubber density, and ρ_f is the foam density.

The cell wall thickness, δ, of NR foams was calculated using equation (2):

$$\delta = d\left[\frac{1}{\sqrt{1 - \frac{\rho_f}{\rho_r}}} - 1\right] \quad (2)$$

3 Results and discussion

3.1 Curing behavior

Figure 1 shows the curing plots of all samples at 90°C and 140°C. The Y-axis in this figure is the difference between the minimum torque, M_L, and maximum torque, M_H, in the ODR test. As can be seen, the compounds at 90°C were not cured until 30 min, and the torque for all samples was close to zero. However, at 140°C, the materials cured at different rates. By addition of silica content from 0 to 40 phr, torque was enhanced due to increased viscosity from the added nanofiller.

The degree of conversion for all samples was calculated as follows:

$$\alpha(t) = \frac{M_t - M_L}{M_H - M_L} \quad (3)$$

where M_t is the torque value at time t. Figure 2 displays the conversion curves of samples at 140°C. As can be seen, the curing reaction of foam samples (S0–S40) was

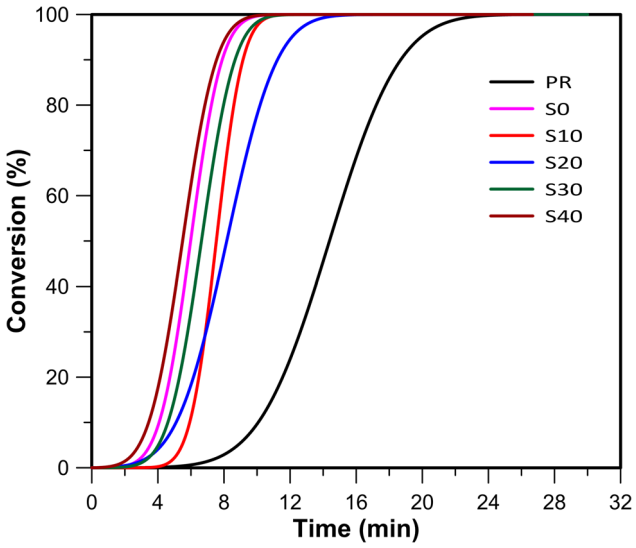

Figure 2: Degree of conversion vs time at 140°C.

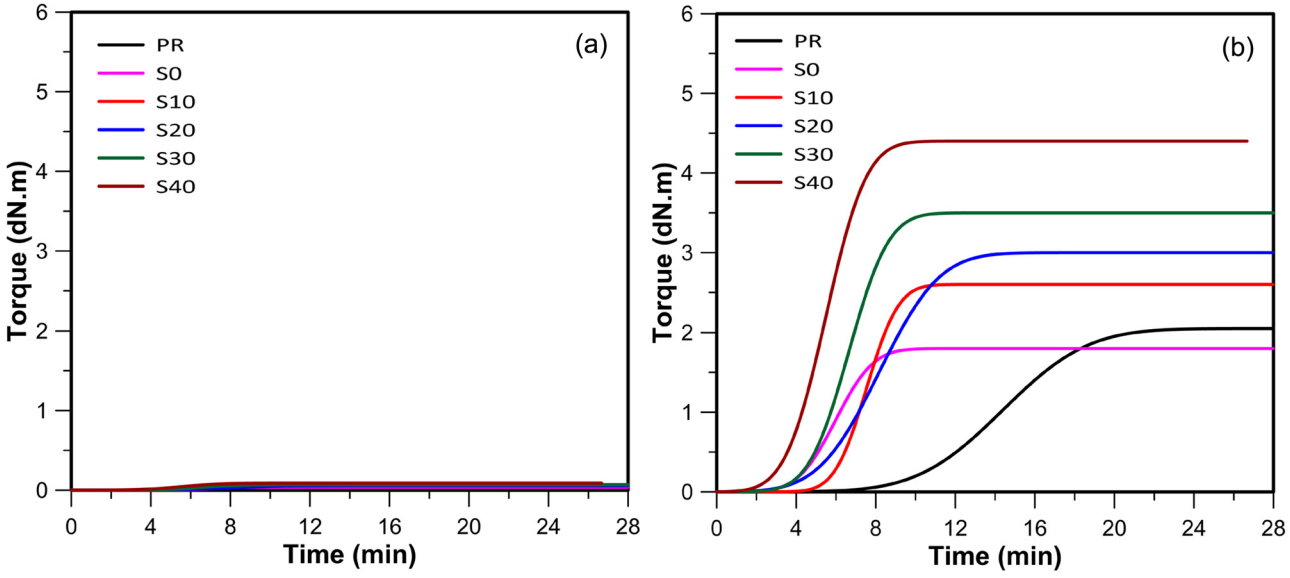

Figure 1: Torque vs time at (A) 90°C and (B) 140°C.

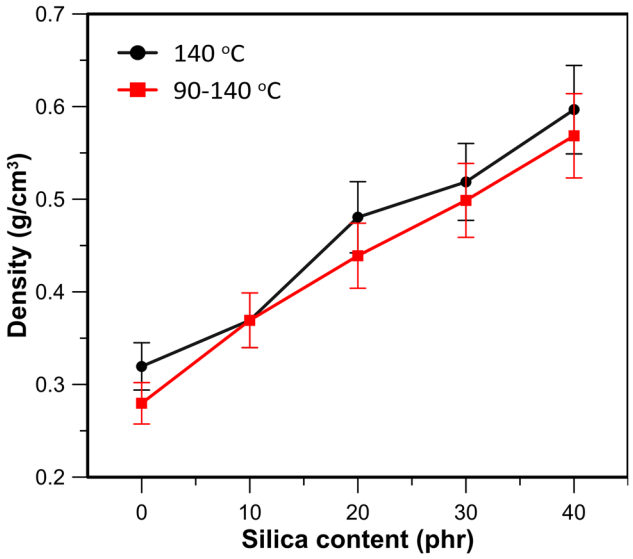

Figure 3: Density of natural rubber composites vs silica content.

faster than the PR (non-foam) sample. This result was due to the exothermic decomposition of blowing agent that accelerated the curing reaction of rubber [56]. The torque for the PR sample was slightly higher than S0 because S0 was a foam, while PR was not; therefore, the finial modulus of PR was higher. Nonetheless, the scorch time and curing time of SX were explicitly lower than PR. This observation confirmed that the addition of nanofiller had a negligible impact on the curing reaction, while the blowing agent clearly promoted curing [56].

3.2 The density of foams

Figure 3 shows the density of the foams versus silica content for different foam processing. The addition of silica content up to 40 phr increased the foam density from approximately 0.3 to 0.6 g/cm^3. This result might be related to the higher density of mineral particle when compared with the natural rubber. Moreover, compounds containing a higher silica level had higher viscosity (Figure 1b), which could restrict the bubble growth. However, the densities of samples from the two-step foaming process were 7% to 22% lower than foams prepared in one-step at 140°C. In two-step foaming, bubbles first grew and then the rubber cured. Thus, there was no limitation such as crosslinking on the bubble growth.

Viscosity, which is a barrier to cell growth, was higher at 90°C when compared with 140°C. Therefore, the bubble growth rate might be slower in the two-step foaming process. However, the curing reaction did not occur at 90°C. As the curing reaction progressed, the viscosity increased and bubble growth was prevented. The scorch time of samples at 140°C was between 3 and 7 min (Figure 2). Hence, in the one-step foaming at 140°C, bubbles had less time to grow and foams with higher density were produced.

3.3 Microscopic analysis

Figure 4 shows the cell structure of samples foamed by one-step and two-step foaming. According to the SEM

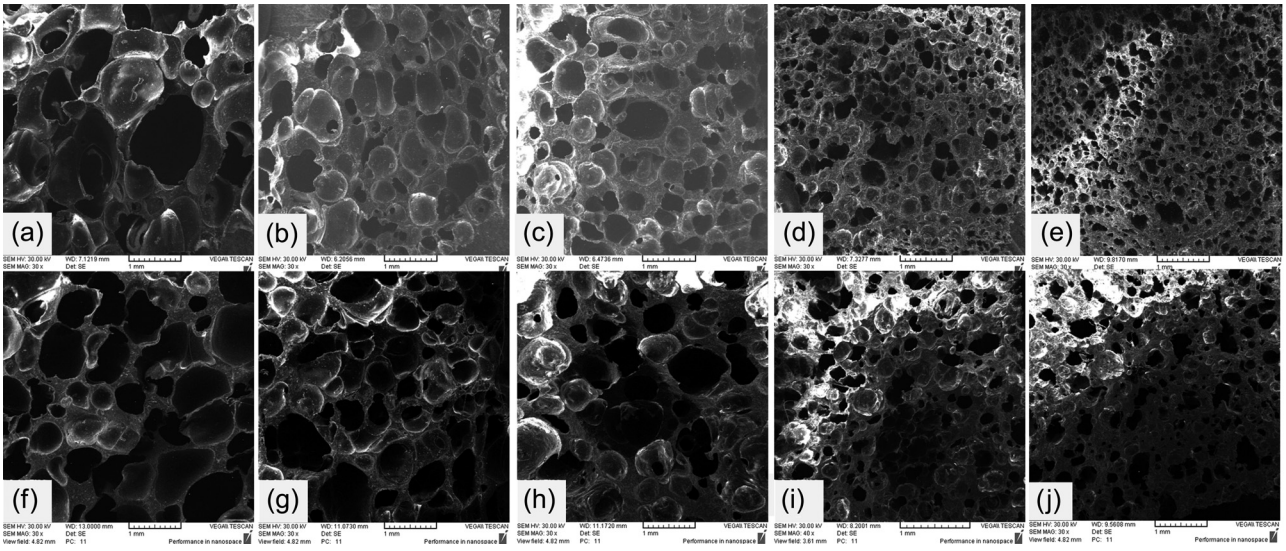

Figure 4: SEM images of NR foams prepared at 140°C (a) S0, (b) S10, (c) S20, (d) S30, and (e) S40 and prepared at 90–140°C (f) S0, (g) S10, (h) S20, (i) S30, and (j) S40 (scale bar: 1 mm).

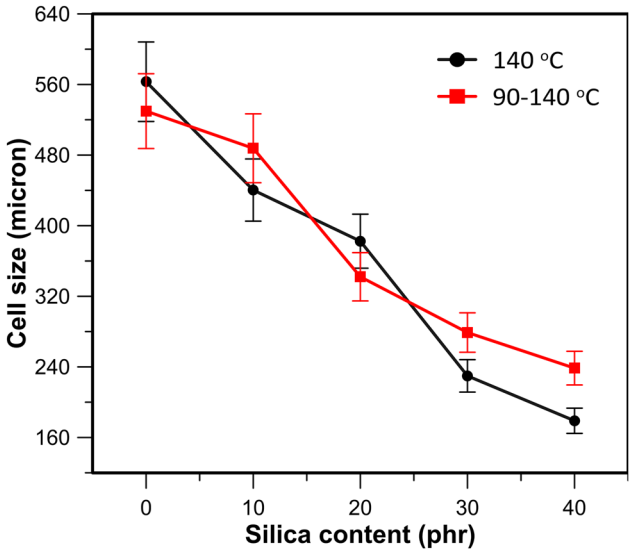

Figure 5: Variation of average cell diameter and its deviation in different foams.

figures, many closed cells in addition to a few open cells were observed. The addition of silica resulted in smaller cell size and more uniform distribution. However, the cell diameter from the two-step foaming process was not uniform and was larger when compared with the one-step foaming. Additionally, cell coalescence even at 40 phr silica appeared. Apparently, natural rubber at 90°C does not have enough strength to hold the gas inside bubbles and prevent cell coalescence over a long time.

Figure 5 illustrates the cell size of samples versus silica content. A higher silica content led to a lower cell diameter. For instance, the cell size of S0, which excluded silica, was about 580 µm, while for S40 the cell size was 200 µm. The cell sizes of foams prepared by route 1 were between 15% and 30% smaller than foams prepared by route 2.

Figures 6 and 7 show the prepared cell size distribution of foams prepared by routes 1 (one-step) and 2 (two-step), respectively. As seen, adding silica resulted in a smaller cell size and a narrower and more uniform cell distribution.

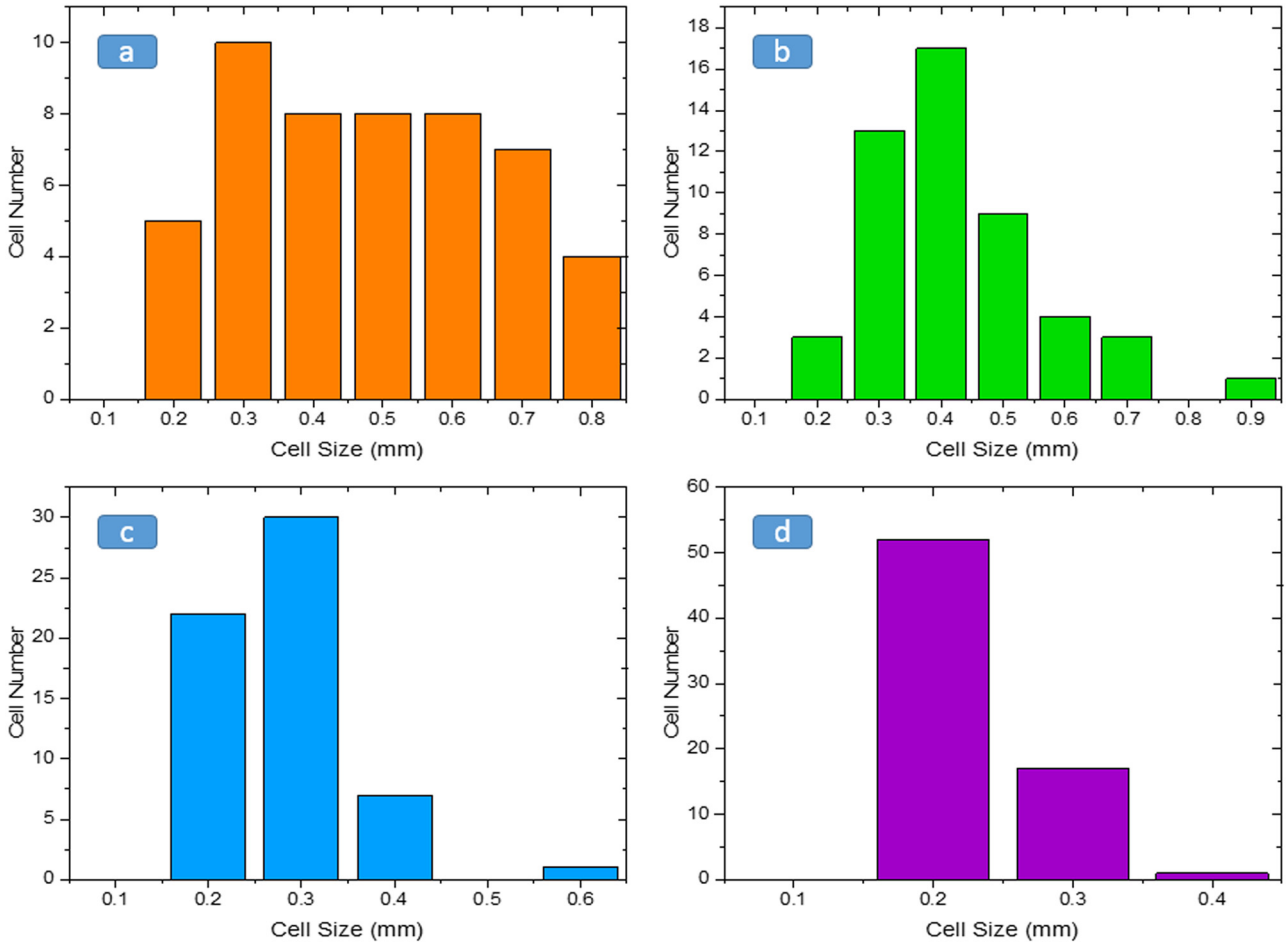

Figure 6: Distribution of cell size of foams prepared by route 1: (a) S10, (b) S20, (c) S30, and (d) S40.

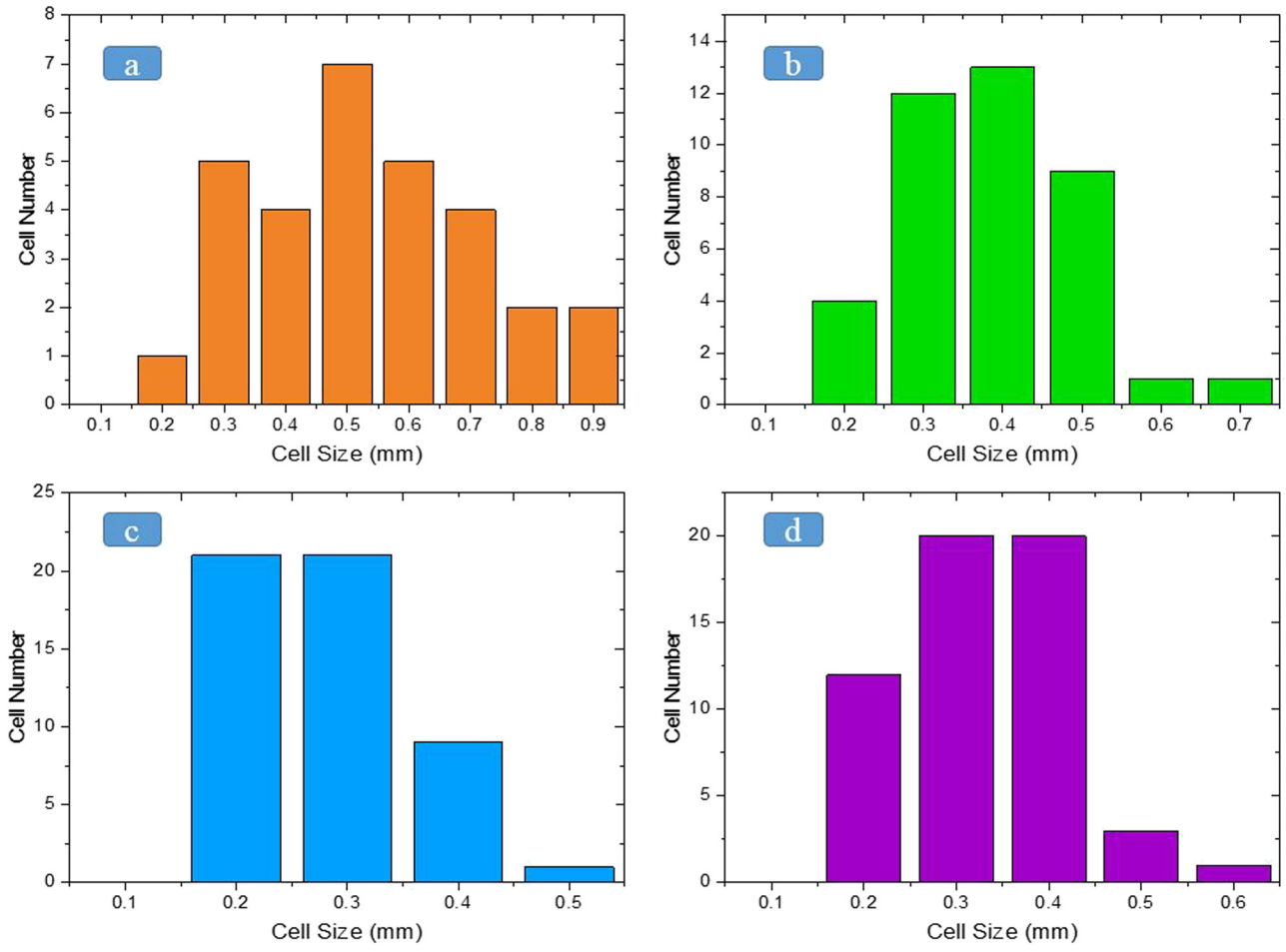

Figure 7: Distribution of cell size of foams prepared by route 2: (a) S10, (b) S20, (c) S30, and (d) S40.

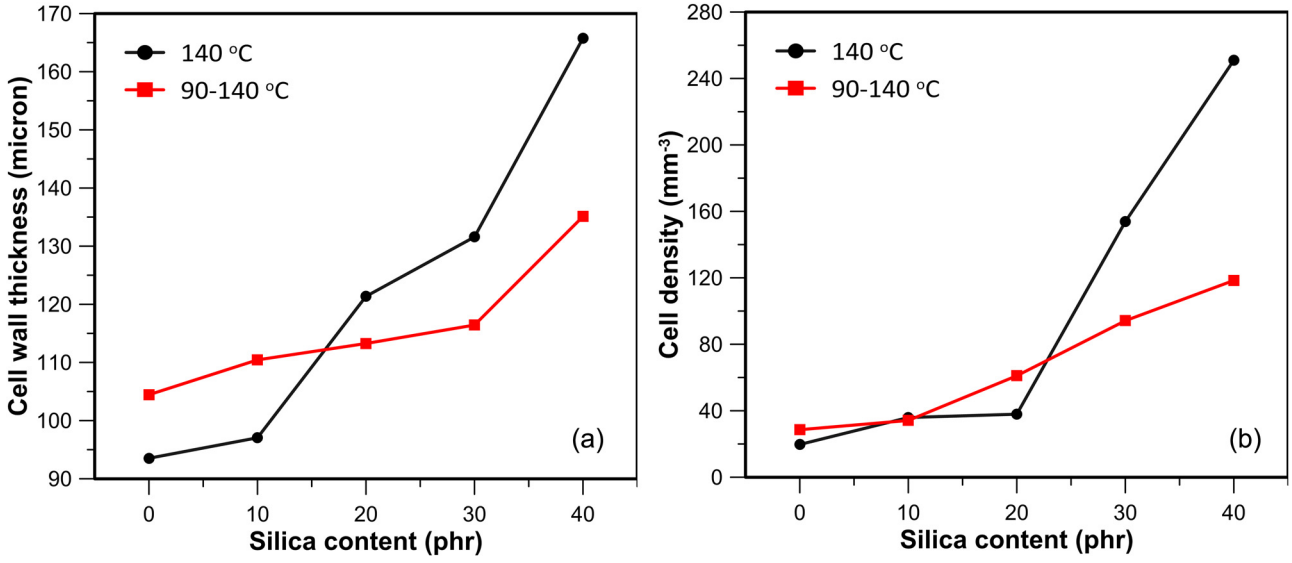

Figure 8: Variation of (a) cell wall thickness and (b) cell density of NR foams.

On the other hand, the cell density and cell wall thickness increased by adding silica due to the nucleating effect of silica particles (Figure 8). The cell density of S40 prepared by route 1 was approximately 10-fold higher than S0 and two-fold higher than S40 prepared by route 2. Therefore, the performance of silica as a nucleating agent in route 2 was inferior due to the lower temperature providing less energy for nucleation.

4 Conclusions

The curing and cell structure of natural rubber filled silica composite foams prepared by one-step and two-step foaming processes were compared. The addition of blowing agent to the NR compound noticeably promoted the curing rate and lessened the scorch time. The presence of silica had a negligible impact on the curing behavior. Two-step foaming caused a decrease in foam density and an increase in cell density. Moreover, the two-step foaming route caused the larger cell size and nonuniform cell distribution. The average cell size from route 1 was 15–30% lesser than route 2. At the higher temperature, faster curing restricted the bubble growth. In contrast, unstable grown bubbles at 90°C due to the lack of curing generated larger cells with a nonuniform distribution along with increased cell coalescence.

Acknowledgments: The authors would like to thank the Iran National Science Foundation (INSF) for financial support of this study.

Conflict of interest: The authors declare no conflict of interest regarding the publication of this paper.

References

[1] Roy S, Petrova RS, Mitra S. Effect of carbon nanotube (CNT) functionalization in epoxy-CNT composites. Nanotechnol Rev. 2018;7:475–85.
[2] Zare Y, Rhee K. Evaluation and development of expanded equations based on Takayanagi model for tensile modulus of polymer nanocomposites assuming the formation of percolating networks. Phys Mesomechanics. 2018;21:351–7.
[3] Kim S, Zare Y, Garmabi H, Rhee KY. Variations of tunneling properties in poly (lactic acid)(PLA)/poly (ethylene oxide)(PEO)/carbon nanotubes (CNT) nanocomposites during hydrolytic degradation. Sens Actuators A: Phys. 2018;274:28–36.
[4] Zare Y, Rhee KY. Modeling of viscosity and complex modulus for poly (lactic acid)/poly (ethylene oxide)/carbon nanotubes nanocomposites assuming yield stress and network breaking time. Compos Part B: Eng. 2019;156:100–7.
[5] Zare Y, Rhee KY, Park S-J. A developed equation for electrical conductivity of polymer carbon nanotubes (CNT) nanocomposites based on Halpin-Tsai model. Results Phys. 2019;14:102406.
[6] Naseer B, Srivastava G, Qadri OS, Faridi SA, Islam R, Younis K. Importance and health hazards of nanoparticles used in the food industry. Nanotechnol Rev. 2018;7:623–41.
[7] Chen W, Lv G, Hu W, Li D, Chen S, Dai Z. Synthesis and applications of graphene quantum dots: A review. Nanotechnol Rev. 2018;7:157–85.
[8] Zare Y, Rhim S, Garmabi H, Rhee KY. A simple model for constant storage modulus of poly (lactic acid)/poly (ethylene oxide)/carbon nanotubes nanocomposites at low frequencies assuming the properties of interphase regions and networks. J Mech Behav Biomed Mater. 2018;80:164–70.
[9] Zare Y, Rhee KY. Tensile strength prediction of carbon nanotube reinforced composites by expansion of cross-orthogonal skeleton structure. Compos Part B: Eng. 2019;161:601–7.
[10] Zare Y, Rhee KY. A simulation work for the influences of aggregation/agglomeration of clay layers on the tensile properties of nanocomposites. JOM. 2019;71:3989–95.
[11] Zare Y, Rhee KY. A multistep methodology for calculation of the tensile modulus in polymer/carbon nanotube nanocomposites above the percolation threshold based on the modified rule of mixtures. RSC Adv. 2018;8:30986–93.
[12] Rajaee P, Ghasemi FA, Fasihi M, Saberian M. Effect of styrene-butadiene rubber and fumed silica nano-filler on the microstructure and mechanical properties of glass fiber reinforced unsaturated polyester resin. Compos Part B: Eng. 2019;173:106803.
[13] Ajorloo M, Fasihi M, Ohshima M, Taki K. How are the thermal properties of polypropylene/graphene nanoplatelet composites affected by polymer chain configuration and size of nanofiller? Mater Des. 2019;181:108068.
[14] Khoramishad H, Khakzad M, Fasihi M. The effect of outer diameter of multi-walled carbon nanotubes on fracture behavior of epoxy adhesives. Sci Iran, Trans B, Mech Eng. 2017;24:2952–62.
[15] Zhang P, Yi W, Xu H, Gao C, Hou J, Jin W, Lei Y, Hou X. Supramolecular interactions of poly [(9, 9-dioctylfluorenyl-2, 7-diyl)-co-thiophene] with single-walled carbon nanotubes. Nanotechnol Rev. 2018;6:221–31.
[16] Ban I, Stergar J, Maver U. NiCu magnetic nanoparticles: review of synthesis methods, surface functionalization approaches, and biomedical applications. Nanotechnol Rev. 2018;7:187–207.
[17] Zare Y, Park SP, Rhee KY. Analysis of complex viscosity and shear thinning behavior in poly (lactic acid)/poly (ethylene oxide)/carbon nanotubes biosensor based on Carreau–Yasuda model. Results Phys. 2019;13:102245.
[18] Razavi R, Zare Y, Rhee KY. The roles of interphase and filler dimensions in the properties of tunneling spaces between CNT in polymer nanocomposites. Polym Compos. 2019;40:801–10.
[19] Rostami A, Vahdati M, Nazockdast H. Unraveling the localization behavior of MWCNTs in binary polymer blends using thermodynamics and viscoelastic approaches. Polym Compos. 2018;39:2356–67.

[20] Rostami A, Vahdati M, Alimoradi Y, Karimi M, Nazockdast H. Rheology provides insight into flow induced nano-structural breakdown and its recovery effect on crystallization of single and hybrid carbon nanofiller filled poly (lactic acid). Polymer. 2018;134:143–54.
[21] Seyfoori A, Ebrahimi SS, Omidian S, Naghib SM. Multifunctional magnetic $ZnFe_2O_4$-hydroxyapatite nanocomposite particles for local anti-cancer drug delivery and bacterial infection inhibition: an in vitro study. J Taiwan Inst Chem Eng. 2019;96:503–8.
[22] Mamaghani KR, Naghib SM. The effect of stirring rate on electrodeposition of nanocrystalline nickel coatings and their corrosion behaviors and mechanical characteristics. Int J Electrochem Sci. 2017;12:5023–35.
[23] Kalantari E, Naghib SM. A comparative study on biological properties of novel nanostructured monticellite-based composites with hydroxyapatite bioceramic. Mater Sci Eng: C. 2019;98:1087–96.
[24] Kalantari E, Naghib SM, Naimi-Jamal MR, Aliahmadi A, Iravani NJ, Mozafari M. Nanostructured monticellite for tissue engineering applications-Part I: Microstructural and physicochemical characteristics. Ceram Int. 2018;44:12731–8.
[25] Kalantari E, Naghib SM, Iravani NJ, Aliahmadi A, Naimi-Jamal MR, Mozafari M. Nanostructured monticellite for tissue engineering applications–Part II: Molecular and biological characteristics. Ceram Int. 2018;44:14704–11.
[26] Kalkhoran AHZ, Naghib SM, Vahidi O, Rahmanian M. Synthesis and characterization of graphene-grafted gelatin nanocomposite hydrogels as emerging drug delivery systems. Biomed Phys Eng Express. 2018;4:055017.
[27] Power AC, Gorey B, Chandra S, Chapman J. Carbon nanomaterials and their application to electrochemical sensors: a review. Nanotechnol Rev. 2018;7:19–41.
[28] Ventrapragada LK, Creager SE, Rao AM, Podila R. Carbon nanotubes coated paper as current collectors for secondary Li-ion batteries. Nanotechnol Rev. 2019;8:18–23.
[29] Li Z, Xu K, Pan Y. Recent development of supercapacitor electrode based on carbon materials. Nanotechnol Rev. 2019;8:35–49.
[30] Li Z, Xu K, Wei F. Recent progress on photodetectors based on low dimensional nanomaterials. Nanotechnol Rev. 2018;7:393–411.
[31] Zare Y, Rhee KY, Park S-J. A modeling methodology to investigate the effect of interfacial adhesion on the yield strength of MMT reinforced nanocomposites. J Ind Eng Chem. 2019;69:331–7.
[32] Zare Y, Rhee KY. Evaluation of the tensile strength in carbon nanotube-reinforced nanocomposites using the expanded Takayanagi model. JOM. 2019;71:3980–8.
[33] Zare Y, Rhee KY. Effects of interphase regions and filler networks on the viscosity of PLA/PEO/carbon nanotubes biosensor. Polym Compos. 2019;40:4135–41.
[34] Zare Y, Rhee KY, Park S-J. Modeling the roles of carbon nanotubes and interphase dimensions in the conductivity of nanocomposites. Results Phys. 2019;15:102562.
[35] Naghib SM. Two dimensional functionalized methacrylated graphene oxide nanosheets as simple and inexpensive electrodes for biosensing applications. Micro Nano Lett. 2019;14:462–5.
[36] Naghib SM, Parnian E, Keshvari H, Omidinia E, Eshghan-Malek M. Synthesis, characterization and electrochemical evaluation of polyvinylalchol/graphene oxide/silver nanocomposites for glucose biosensing application. Int J Electrochem Sci. 2018;13:1013–26.
[37] Rostami A, Moosavi MI. High-performance thermoplastic polyurethane nanocomposites induced by hybrid application of functionalized graphene and carbon nanotubes. J Appl Polym Sci. 2019;137:48520.
[38] Rostami A, Eskandari F, Masoomi M, Nowrouzi M. Evolution of microstructure and physical properties of PMMA/MWCNTs nanocomposites upon the addition of organoclay. J Oil, Gas Petrochem Technol. 2019;6(1):28–38.
[39] Joseph R, Eaves D. Handbook of polymer foams. UK: Rapra Technology; 2004.
[40] Moon S, Jo B, Farris RJ. Flame resistance and foaming properties of NBR compounds with halogen-free flame retardants. Polym Compos. 2009;30:1732–42.
[41] Choi SS, Park BH, Song H. Influence of filler type and content on properties of styrene-butadiene rubber (SBR) compound reinforced with carbon black or silica. Polym Adv Technol. 2004;15:122–7.
[42] Adachi H, Hasegawa T, Asano T. Cell distributions in and sound absorption characteristics of flexible polyurethane foams. J Appl Polym Sci. 1997;65:1395–402.
[43] Watcharakul S, Umsakul K, Hodgson B, Chumeka W, Tanrattanakul V. Biodegradation of a blended starch/natural rubber foam biopolymer and rubber gloves by Streptomyces coelicolor CH13. Electron J Biotechnol. 2012;15:8.
[44] Vahidifar A, Nouri Khorasani S, Park CB, Naguib HE, Khonakdar HA. Fabrication and characterization of closed-cell rubber foams based on natural rubber/carbon black by one-step foam processing. Ind & Eng Chem Res. 2016;55:2407–16.
[45] Ramasamy S, Ismail H, Munusamy Y. Effect of rice husk powder on compression behavior and thermal stability of natural rubber latex foam. BioResources. 2013;8:4258–69.
[46] Rathnayake I, Ismail H, Azahari B, Darsanasiri ND, Rajapakse S. Synthesis and characterization of nano-silver incorporated natural rubber latex foam. Polym Technol Eng. 2012;51:605–11.
[47] Najib N, Ariff Z, Bakar A, Sipaut C. Correlation between the acoustic and dynamic mechanical properties of natural rubber foam: Effect of foaming temperature. Mater Des. 2011;32:505–11.
[48] Harnnarongchai W, Chaochanchaikul K. Effect of blowing agent on cell morphology and acoustic absorption of natural rubber foam. Appl Mech Mater. 2015;123:25–9.
[49] Ariff Z, Zakaria Z, Tay L, Lee S. Effect of foaming temperature and rubber grades on properties of natural rubber foams. J Appl Polym Sci. 2008;107:2531–8.
[50] Kim J-H, Choi K-C, Yoon J-M. The foaming characteristics and physical properties of natural rubber foams: effects of carbon black content and foaming pressure. J Ind Eng Chem. 2006;12:795–801.
[51] Pechurai W, Muansupan T, Seawlee P. Effect of foaming temperature and blowing agent content on cure characteristics, mechanical and morphological properties of natural rubber foams. Adv Mater Res. 2014;113:454–7.
[52] Sritapunya T. Study on preparation and properties of foam rubber from natural rubber ribbed smoked sheet using salt of

amino alcohol and carbonic acid as foaming agent. Adv Mater Res. 2014;117:115–8.
[53] Najib N, Ariff Z, Manan N, Bakar A, Sipaut C. Effect of blowing agent concentration on cell morphology and impact properties of natural rubber foam. J Phys Sci. 2009;20: 13–25.
[54] Charoeythornkhajhornchai P, Samthong C, Boonkerd K, Somwangthanaroj A. Effect of azodicarbonamide on microstructure, cure kinetics and physical properties of natural rubber foam. J Cell Plast. 2017;53:287–303.
[55] Bayat H, Fasihi M. Effect of coupling agent on the morphological characteristics of natural rubber/silica composites foams. e-Polymers. 2019;19:430–6.
[56] Bayat H, Fasihi M. Curing characteristics and cellular morphology of natural rubber/silica composite foams. Polym Bull. 2019;1–14.